Available online at www.sciencedirect.com
ScienceDirect
ELSEVIER
Photonics and Nanostructures – Fundamentals and Applications 8 (2010) 7–13
PHOTONICS AND NANOSTRUCTURES
Fundamentals and Applications
www.elsevier.com/locate/photonics

Nanoscale plasmonic devices for dynamically controllable beam focusing and scanning

A.E. Çetin [a,b], A. Sennaroglu [c,d,*], Ö.E. Müstecaplıoğlu [c,e]

[a] *Photonics Center, Boston University, Boston, MA 02215, USA*
[b] *School of Electrical and Computer Engineering, Boston University, Boston, MA 02215, USA*
[c] *Department of Physics, Koç University, Sarıyer, İstanbul 34450, Turkey*
[d] *Department of Electrical and Computer Engineering, Koç University, Sarıyer, İstanbul 34450, Turkey*
[e] *Institute of Quantum Electronics, ETH Zurich, 8093 Zurich, Switzerland*

Received 23 September 2009; received in revised form 24 November 2009; accepted 1 December 2009
Available online 23 December 2009

Abstract

We have performed simulations to investigate the variable focusing and scanning capability of metallic nano-slit configurations. In a symmetric nanorod configuration inside an aperture with adjustable offset of the center rod, the focal position is found to be variable in the 0.5–3.5 μm range. In a ladder configuration of the rods, the transmitted beam is found to be deflected up to 23°. Horizontal displacement of rods allows for finer control of angular scanning up to 4°. Such slit geometries offer the potential to be controlled by using nano-positioning systems for applications in dynamic beam shaping and scanning on the nanoscale.

PACS : 78.67.−n; 68.37.Uv; 73.20.Mf

Keywords: Plasmonics; Metallic nano-optic lenses; Beam shaping; Nano-scanner; Beam deflection

1. Introduction

One of the most promising applications of nano-optic devices involves nanoscale control of light [1–8] by use of nano-lenses, which are slits of subwavelength size embedded in metal layers. Studies of light transmission through such subwavelength apertures suggest a variety of functions such as beam focusing and scanning at the nanoscale, enabling the development of devices for ultra high-density data storage architectures as well as near-field microscopy and nano-scanning. Nano-lenses operate on the principle of extraordinary light transmission (EOT) according to which surface plasmon (SP) resonances enable enhanced optical transmission of light through a subwavelength aperture. In practical applications, it is often desirable to vary the focusing and deflection characteristics of the nano-lenses in a fast and controllable way. In previous studies, Sun and Kim employed finite-difference time domain simulations to show that nano-slit array structures on a metal layer with tapered film thickness can be used for beam shaping and tilting. In particular, their simulations show that the focal length of the convex-shaped array can be varied by changing the number of slits [3]. In another study, Min et al. proposed a new method for beam shaping and tilting by using slit structures filled with nonlinear dielectric media and showed that the deflection angle and the focus length can be controlled

* Corresponding author at: Department of Physics, Koç University, Sarıyer, İstanbul 34450, Turkey. Tel.: +90 212 338 14 29.
E-mail addresses: acetin@bu.edu (A.E. Çetin), asennar@ku.edu.tr (A. Sennaroglu), omustecap@ku.edu.tr (O.E. Müstecaplıoğlu).

1569-4410/$ – see front matter
doi:10.1016/j.photonics.2009.12.001

by the intensity of the incident light beam [9]. While both of the proposed methods provide valuable means of focus and deflection control, they are complicated by the fact that changing the number of slits dynamically is difficult and adding a nonlinear medium increases the complexity of the structure.

In this Paper, we extend the previous studies and examine ways of controlling the focus location and the deflection angle of the transmitted beam by varying the geometrical configuration of the nano-slit structure. Although the original idea is already proposed by Sun and Kim [3], we simplified the configuration of nano-scanner from the array of stepwise metal to the array of nanorods. This approach, which could, in principle, utilize the recently developed nano-positioning concepts based on energy-scavenging piezoelectric positioning systems [10–13] could lead to faster dynamic control of the transmitted beam parameters. In the simulations, we used the actual dielectric response function data for silver to perform electromagnetic analysis of nanoscale metallic rods for applications in beam focusing and scanning. In particular, we examined the metallic nano-optic lens due to its advantage of being free from the diffraction effects, unlike the conventional dielectric lenses, as was also pointed out in Ref. [3]. Numerical simulations were performed by using COMSOL Multiphysics program. In the Paper, we investigate three different configurations. In the first case, we show that a series of convex-shaped silver nanorods positioned symmetrically inside an aperture can be used to focus the light beam. In addition, varying the offset of the middle rod without breaking the slit symmetry leads to an adjustable focal length. In the second set of simulations, we analyzed the scanning characteristics of the three-rod structure configured in the shape of a ladder. By reversing the ladder direction, the simulations show that the transmitted beam can be deflected up to about 23° to either side of the original propagation direction. Finally, we show that via lateral displacement of the convex-shaped nanorods, finer beam scanning can be achieved up to deflection angles of approximately 4°. In Section 5, we also provide a simple, physical model based on scalar diffraction theory to justify the feasibility of using displaced rod configuration for beam deflection.

2. Controlling the focusing power of nano-lenses

In the first part of the simulations, we investigated the focusing characteristics of convex-shaped, nanorod structures. As shown in Fig. 1(a), the particular structure

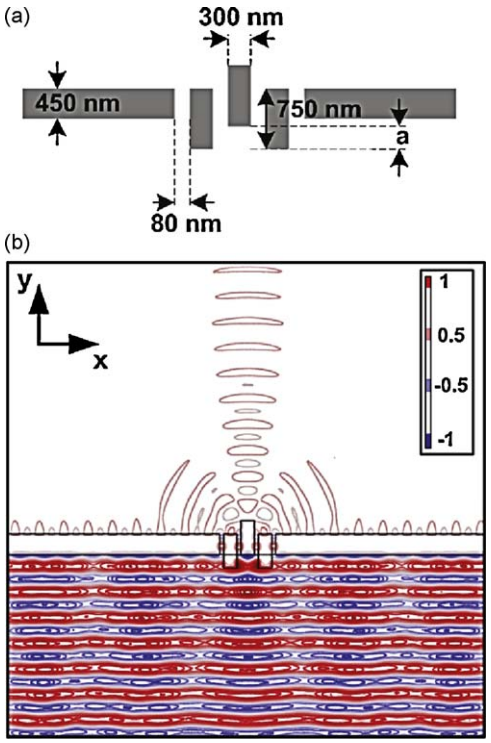

Fig. 1. Beam focusing by a nano-scanner with movable slits. (a) The geometry and dimensions of the metallic nano-scanner under consideration are shown. (b) COMSOL Multiphysics simulation of focusing beam with silver ($\varepsilon = -11.66 + i0.3771$ at $\lambda = 561$ nm) nano-scanner where the slits are located to make a convex shape. A TM plane wave with wavelength of 561 nm is incident at the bottom side of the system. Figure shows a snapshot of the H_z distribution in the system when $a = 300$ nm.

we studied consists of a silver layer with a thickness of 450 nm and a 1220-nm-wide aperture containing three, equally spaced, silver rods each with a thickness of 300 nm and height of 750 nm. In the COMSOL Multiphysics simulations, the dielectric response function was assumed to be equal to the empirical value ($\varepsilon = -11.66 + i0.3771$) for silver [14] at the wavelength of 561 nm. Initially, the three-rods were configured in a convex shape with $a = 300$ nm (see Fig. 1(a)). In the calculations, we assumed that a transverse-magnetic (TM) plane wave with a wavelength of 561 nm was incident at the bottom side of the metallic structure. In COMSOL Multiphysics simulations, we adjusted the boundary conditions to make the system infinite in the x-direction. Fig. 1(b) shows a snapshot of the z-component of the electromagnetic field (H_z) when $a = 300$ nm. As can be seen, the wave emanating from the slits is first brought to a focus before starting to diverge. In order to determine the focus location f, we first calculated the spot-size function $w(y)$ at each y

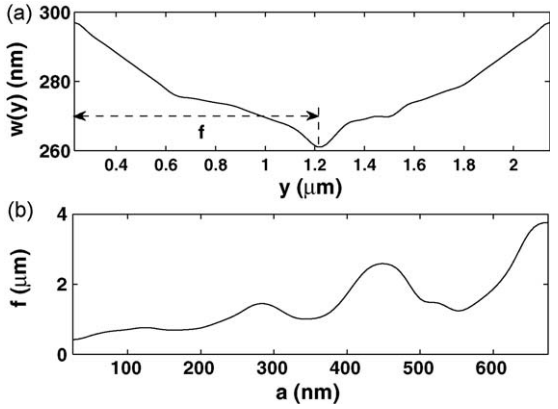

Fig. 2. Controlling focal point of the transmitted beam by a nano-scanner. (a) The spot-size function of the nano-scanner which has the dimension shown in Fig. 1(a) when $a = 300$ nm. (b) The focus length of the system as a function of a.

value. $w(y)$ corresponds to the spatial separation between the $1/e^2$ points of the maximum axial intensity.

Fig. 2(a) shows the calculated variation of $w(y)$ as a function of y. Note that the spot-size reaches a local minimum of 261 nm after a distance of 1.22 μm when $a = 300$ nm. It is also of interest to see whether the slit geometry can be modified in a way to control the focus location f. To test this, we simulated the effect of the nano-slit structure on the transmission of the TM wave for the case where the middle silver rod has a variable spatial offset shown as the distance a in Fig. 1(a). The simulation results show that when a is varied from 0 to 650 nm, f increases from 0.5 to 3.5 μm. As can be seen from Fig. 2(b), the increase in f is not monotonic, rather, oscillatory behavior is observed possibly due to the complex role of plasmonic resonances. In practice, nano-positioning of the rods to control the focus location can be achieved by using piezoelectric transducers. A piezoelectric motor works on the principle that a change in the shape of the piezoelectric material occurs depending on the strength of the applied electric field. Piezoelectric motors can produce either linear or rotary motion on the nanoscale. Furthermore, they can potentially be self-powered by incorporating nanoscale energy-scavenging systems such as the aligned ZnO nano-wire arrays which have been shown to convert mechanical or acoustic energy to electrical energy [10–13].

3. Beam deflection for wider angle range with vertically movable nanorods

Another important application of nano-slits is beam scanning. This would be of great utility in high-density memory applications where the probe beam can be directed to different memory addresses by a nano-scanner. We analyzed the scanning characteristics of the same nano-slit structure as above at the wavelength of 561 nm. Two geometries were investigated. In the first case, we studied a 'ladder' structure with a step size of 150 nm between consecutive vertically displaced rods. The dimensions of each rod are the same as in Fig. 1(a). The specific geometry of the ladder is further shown in the inset of Fig. 3(a). As can be seen from the snapshot picture of the H_z field, a plane TM wave incident from the bottom side is deflected by an angle of 23.5° to the left of the original propagation direction. If the rods move down as one goes from left to right (see Fig. 3(b)), this time the transmitted beam is deflected by the same amount but in the opposite sense. By going to

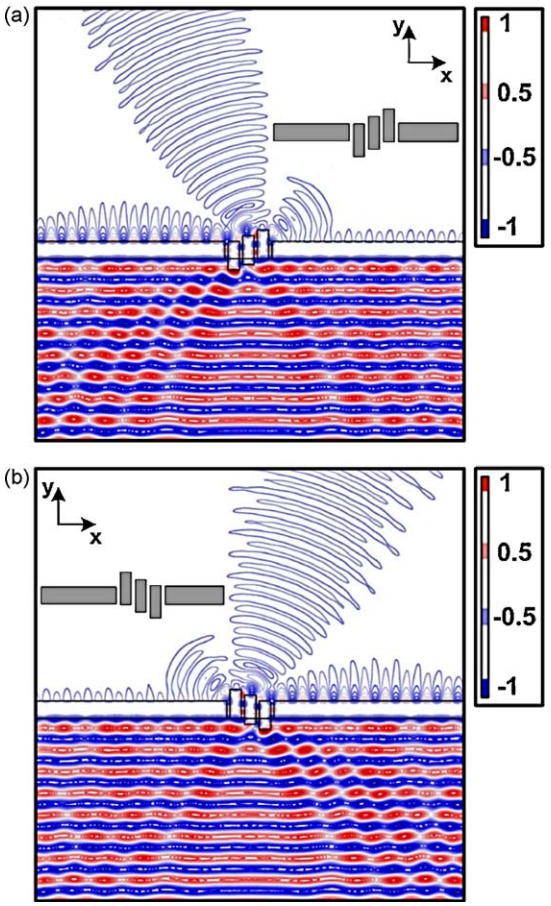

Fig. 3. Beam deflection by a nano-scanner with movable slits. COMSOL Multiphysics simulation of tilting the focused beam with silver ($\varepsilon = -11.66 + i0.3771$ at $\lambda = 561$ nm) nano-lens where the slits are moved vertically between two metal layers is shown. Figure shows a snapshot of the H_z distribution in the system when the slits are moved into different positions. A TM plane wave with wavelength of 561 nm is incident at the bottom side of the system.

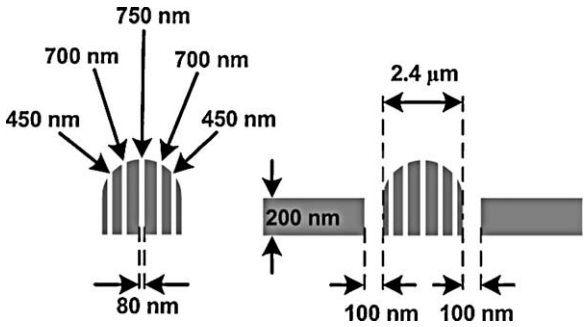

Fig. 4. The geometry and dimensions of the metallic nano-scanner for small angular range consideration.

intermediate configurations between these two extremes, the transmitted beam can be scanned with a full angular sweep of approximately 23°. Having the ability to scan the beam over nanometer-long distances could lead to the development of nanoscale readers for high-density memories.

4. Beam deflection for narrower angle range with horizontally movable convex lens

Finally, our simulations show that it is also possible to achieve finer scanning control of the beam by displacing the convex structure within the aperture. The detailed dimensions of the rods are given in Fig. 4.

Again, the slits are assumed to be silver and the wavelength of light is taken to be 561 nm. For the slit structure which is symmetric about the mid-point of the aperture, the transmitted beam experiences focusing without angular deflection (Fig. 5(a)). This result can be interpreted as the interference of propagating waves generated via diffraction of the SPs reaching the exits of the nano-apertures. When the convex shape is displaced to the right to break the symmetry, the beam undergoes a tilt of approximately 4.5° as shown in Fig. 5(b). The reason behind this phenomenon is that when the convex metallic structure moves toward right, the slit formed in the left of the convex shape starts to excite SPs and the transmission of light through the slit in that region is enhanced. In the upper side of the metallic nano-optic lens, the transmitted beam enhanced via SP formed in the slit region interferes with the focused beam after the metallic nano-optic lens. Thus, the whole transmitted beam tilts toward the direction in which the convex metallic structure moves.

5. Discussion

The transmission of light through a single slit embedded in a metal layer can be expressed in terms of its magnitude and phase as $T = Ae^{i\phi}$ [3], where

$$A = \frac{\tau_{01}\tau_{12}e^{ik_{sp}h}}{1 + \rho_{01}\rho_{12}e^{i2k_{sp}h}}$$

$$\phi = \phi_{01} + \phi_{02} + k_{sp}h - \theta \tag{1}$$

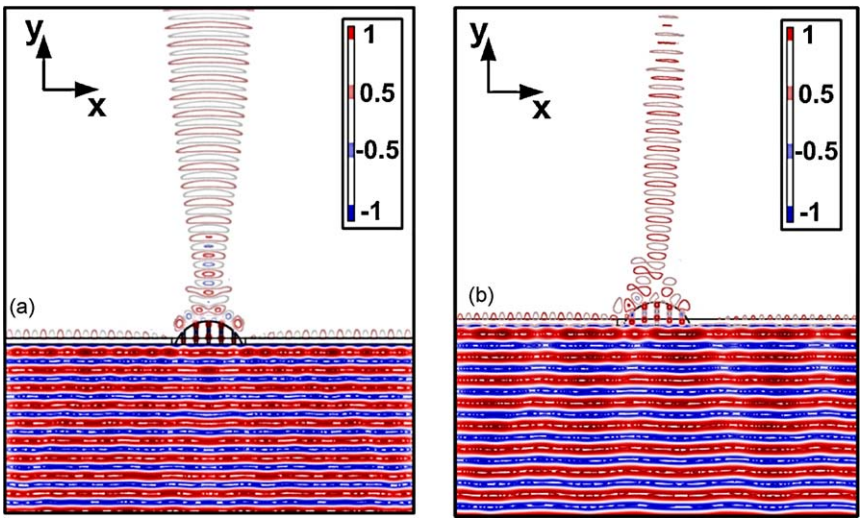

Fig. 5. Small angular range nano-scanning via horizontally moving slits. COMSOL Multiphysics simulation of tilting the focused beam with the metallic nano-optic lens where the convex metallic structure is moved between two metal layers is shown. Figure shows the snapshots of the system (a) when the convex shape is in the middle of the two metal layers and (b) when the convex shape is next to the metal in the right side. In the figure, H_z distribution of the system is shown. A TM plane wave with a wavelength of 561 nm is incident at the bottom side of the system made of silver ($\varepsilon = -11.66 + i0.3771$ at $\lambda = 561$ nm).

Above, k_{sp} is the SP wavevector, h is the slit depth, 0, 1 and 2 denote the media before, inside, and after the nano-slit array, respectively, and $\rho_{01} = (n_0 - n_{sp})/(n_0 + n_{sp})$, $\rho_{12} = (n_{sp} - n_2)/(n_{sp} + n_2)$, $\phi_{01} = \arg[\rho_{01}]$, $\phi_{02} = \arg[\rho_{12}]$, $\tau_{01} = 1 - \rho_{01}$, $\tau_{12} = 1 - \rho_{12}$, $\theta = \arg[1 + \phi_{01}\phi_{12}e^{i2k_{sp}h}]$. Furthermore, n_{sp} is the effective refractive index of the slit region, n_0 and n_2 are the refractive indices of the media outside the slit. For beam deflection at a specific angle γ, overall phase retardation of the system of several slits embedded in metal layer becomes [16].

$$\phi(y) = 2m\pi + \phi(0) - \frac{2\pi}{\lambda_0} y\sin(\gamma) \tag{2}$$

where y is the direction normal to the surface of the metal, λ_0 is the wavelength of free space and m is an integer. Thus, the most important step for beam deflection from a plasmonic device involves a careful optimization of the width and position of each slit in the metal layer [16]. In that sense, what we have done by moving the metallic parts around the nano-slits in our systems, corresponds to a change in the dimension of each slit. Due to the fact that the transmittance of the slit depends on the dimension of the slits, as we move the metallic parts, the amplitude and phase of the transmittance changes for each slit, hence modifying the transmittance of the overall system.

Deflection of the transmitted beam can be analyzed using a simple model based upon Fresnel–Kirchhoff diffraction theory of Fourier optics. Two sides of the slit can be imagined as two line sources of SPs. At the corners, the line sources would emit spherical waves of optical radiation. Geometry of the transmission through the diffracting aperture is shown in Fig. 6.

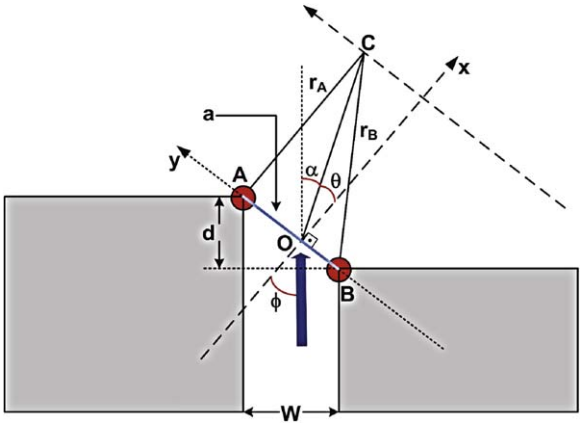

Fig. 6. Diffracting system consisting of a single slit between two metal layers with different heights.

The decay length of the SP is well beyond the step sizes we consider. We assume that both emitters at the corners A and B contribute to the total field with equal field amplitudes ε. On the other hand, the fields will differ in phase by an amount $k_{sp}d$. Denoting the aperture size by $a = \sqrt{w^2 + d^2}$, the total field at the point of observation C can be evaluated in the form of an integral as

$$E_C \propto \frac{1}{i\lambda}\int\int \frac{e^{ikr}}{r}\varepsilon\delta(z) \times \left[\delta\left(y - \frac{a}{2}\right)e^{ik_{sp}d} + \delta\left(y + \frac{a}{2}\right)\right]dydz \tag{3}$$

Here, λ is the wavelength of the transmitted beam in free space and $k = 2\pi/\lambda$. In writing the phase retardation factor between the point sources, we neglected the contributions that might arise due to multiple reflections between the output and input ports of the slit.

Furthermore, we assumed that the phase changes during the excitation of the SP and its annihilation into radiation cancel each other. Having the same media (air) in both input and output ports makes the assumption justified. We are interested in the deflection of the transmitted beam in the far zone relative to the incident one. In the Fraunhofer region the result of the integral is simplified to

$$E_C \propto \frac{2e^{ik(x+((y^2+z^2)/2x))}e^{(ik_{sp}d/2)}}{i\lambda z}\cos\left(\frac{\pi ya}{z\lambda} - \frac{k_{sp}d}{2}\right) \tag{4}$$

In the above expression, coordinates refer to those of the point C. The magnitude squared of the field amplitude can then be expressed in the form

$$|E_C|^2 \propto \frac{4}{(\lambda z)^2}\cos^2\left(\frac{\pi a\sin(\theta)}{\lambda} - \frac{k_{sp}d}{2}\right)$$

by using the angle θ of the transmitted beam to the normal of the aperture surface. It is seen that the intensity maximum will shift from the normal direction to a tilt angle θ determined from $ka\ \sin(\theta) = k_{sp}d$. Introducing $n_{sp} = k_{sp}/k$ and $\varphi = a/d$, we can write an effective Snell's law like relation as $n_{sp}\sin(\varphi) = \sin(\theta)$. The angle of deflection then becomes $\alpha = \varphi - \sin^{-1}(n_{sp}\sin((\varphi))$.

In the multi-slit configuration, a similar expression can be obtained by using the effective dielectric medium approach to model the slits. Calculating the transmission amplitudes and phases (analogous to the Fabry–Perot type of calculation), interference of the fields out of the individual slits can be determined. Note that, in the case of multi-slits, the sources are not the surfaces of the slits but the slits themselves. This is not the case for the single slit discussion presented

above. Beyond rectangular slits, it may be necessary to associate two sources per slit to model oblique apertures of nanorods with finite step sizes.

Both for the single slit analysis discussed above and for the multi-slit configuration, it would be more correct to use superposition of cylindrical waves out of the nano-slits. Besides it is more convenient to use expressions for the magnetic field so that in the Fraunhofer limit one can write the total radiated field as

$$H_z = \sum h_z \frac{e^{ik\rho}}{\sqrt{\rho}} e^{i\delta} \tag{6}$$

where δ is the phase retardation factor of different nano-slit sources and ρ is the radial distance in the xy-plane.

An expression for the complex propagation constant β of the SP confined at the slit surfaces is given to be [17]

$$\tanh\left(\sqrt{\beta^2 - k^2\varepsilon_d}\frac{\omega}{2}\right) = -\frac{\varepsilon_d\sqrt{\beta^2 - k^2\varepsilon_m}}{\varepsilon_m\sqrt{\beta^2 - k^2\varepsilon_d}} \tag{7}$$

The relative dielectric constant for the metal surfaces and the dielectric filling of the slit are respectively denoted by ε_m and ε_d. For simplicity, we assume that the same expression can be used for our case of the slit with an oblique aperture, motivated by the reasoning that the SP is dominantly generated in the rectangular region of the slit.

Let us note that the slits we consider are sufficiently short even with the maximum step size we used, so that the propagation constant can be treated as real. We take $\varepsilon_d = 1$ for the dielectric constant of the air and $\varepsilon_m = -11.66 + i0.3771$ for the dielectric constant of the silver at $\lambda = 561$ nm. Solving Eq. (7), we find $n_{sp} = 1.312$. At the step size of $d = 50$ nm, the incidence angle is $\rho \cong 32^\circ$ and the tilt angle $\theta = 44^\circ$. Thus the deflection is found to be $\alpha = 12^\circ$. COMSOL Multi-physics simulations also indicate that deflection angle 11.78°, in very good agreement.

At higher step sizes such as 150 nm or 300 nm, the above method cannot be applied directly as the incidence angle becomes larger than the critical angle of total internal reflection. A typical simulation result is given in Fig. 7. In this case, multiple scattering events at the slit exit as well as higher order diffraction become significant. To illustrate some of the complications that may arise, we shall give two possible mechanisms that can contribute to the emission pattern in the case of slits with long step sizes.

By geometrical analysis, we have found that the beam can make one internal reflection from the surface of the effective (hypothetical) dielectric and comes back

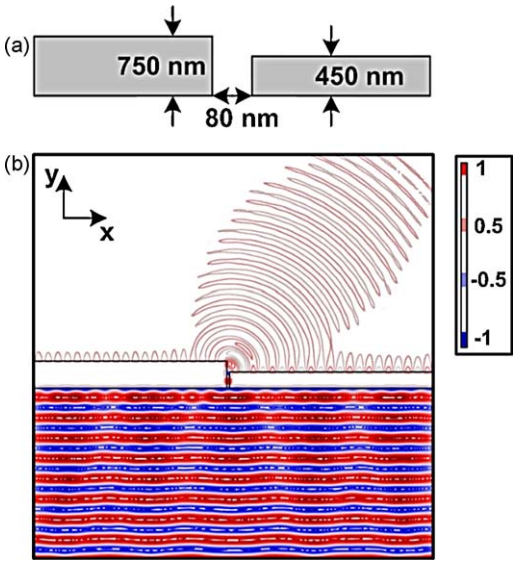

Fig. 7. (a) Dimension of the diffracting system. (b) COMSOL Multi-physics simulation of the deflection of the incident beam by a system consisting of a single slit between two metal layers with different heights. A TM plane wave with wavelength of 561 nm is incident at the bottom side of the system made of silver ($\varepsilon = -11.66 + i0.3771$ at $\lambda = 561$ nm).

with a new angle of incidence $\varphi' = 3\varphi - 180^\circ$. This would be less than the critical angle so that the new deflection angle can be calculated via

$$\alpha' = \varphi - \sin^{-1}(n_{sp}\sin(\varphi')) \tag{8}$$

In addition to internal reflection, higher order diffraction peaks may contribute via the relation

$$\frac{m\lambda}{a} + n_{sp}\sin(\varphi) = \sin(\theta) \tag{9}$$

with m is an integer. When $n_{sp}\sin(\varphi) > 1$, higher order diffraction spots with negative m may reduce $n_{sp}\sin(\varphi)$ below unity. Due to the presence of competing mechanisms, long step size situations are difficult to analyze analytically and estimations become too crude.

Our work indicates a potential link between nanopiezotronics and nano-scanning. We have analyzed two cases of nano-scanning, one with lateral shifts of the nanorod group, and the other with vertical relative shifts of the nanorods. Current experimental efforts allow for controlling lateral motion of metallic nanorods, with dimensions about 40 nm, via atomic force microscope manipulation [18]. Thus our horizontal shift proposal seem to be quite close to current experimental capability. Due to the small distance between the nanorods in our proposal, the vertical relative shift is more challenging experimentally, but

may be possible by using on purpose designed substrates with anisotropic and inhomogeneous piezoelectric layers.

6. Conclusion

In summary, we have investigated the dynamically controllable focusing and scanning capability of metallic nano-slit configurations in which SP enhanced subwavelength light transmission effects can be observed. Three basic nano-slit configurations were analyzed by using numerical computation schemes. A symmetric, three-rod configuration positioned inside an aperture was found to result in beam focusing. In addition, a variable spatial offset of the middle rod led to a variable focal length. Two other configurations were later analyzed to investigate the scanning characteristics of the structure. In particular, our results reveal that controlling the relative vertical positions of the metallic nanorods, for example by forming a ladder configuration, enables beam scanning by up to 23°. Furthermore, horizontal position control of convex-shaped nanorod geometry leads to small angular scanning up to about 4° to either side of the propagation direction. In practice, nano-positioning of the rods may be achieved by use of piezoelectric transducers. Such dynamical control on the beam direction can lead to other applications of nano-lenses such as nano-scanners or can be exploited for high-density memory reading and writing. In combination with the previous ideas on active control of nano-lenses, such as filling the slit region with dielectrics, in particular with nonlinear materials [9], we expect that our results could lead to the realization of optimum designs of nano-lenses [15]. This should play an important role in inspiring new experiments and applications in nanophotonics.

Acknowledgements

A.E. Çetin acknowledges research grants by TÜBİAK (The Scientific and Technological Research Council of Turkey). A. Sennaroglu gratefully acknowledges the research support from the TÜBA (The Turkish Academy of Sciences). The authors are also grateful to M.I. Aksun for many illuminating discussions. Ö.E. Müstecaplıoğlu is grateful to M. Benyoucef for useful discussions and careful remarks on the experimental feasibility of the proposal.

References

[1] L.M. Moreno, F.J.G. Vidal, H.J. Lezec, K.M. Pellerin, T. Thio, J.B. Pendry, T.W. Ebbesen, Phys. Rev. Lett. 86 (2001) 1114.
[2] W.L. Barnes, A. Dereux, T.W. Ebbesen, Nature 424 (2003) 824.
[3] Z. Sun, H.K. Kim, Appl. Phys. Lett. 85 (2004) 642.
[4] R. Gordon, Phys. Rev. B 73 (2006) 153405.
[5] Y.S. Jung, Z. Sun, J. Wuenschell, H.K. Kim, Appl. Phys. Lett. 88 (2006) 243105.
[6] W.L. Barnes, W.A. Murray, J. Dintinger, E. Devaux, T.W. Ebbesen, Phys. Rev. Lett. 92 (2004) 107401.
[7] P. Lalanne, J.P. Hugonin, Nat. Phys. 2 (2006) 551.
[8] P. Lalanne, J.P. Hugonin, J.C. Rodier, Phys. Rev. Lett. 95 (2005) 263902.
[9] C. Min, P. Wang, X. Jiao, Y. Deng, H. Ming, Opt. Express 15 (2007) 9541.
[10] X.D. Wang, J.H. Song, J. Liu, Z.L. Wang, Science 316 (2007) 102.
[11] X.D. Wang, J. Zhou, J.H. Song, J. Liu, N.S. Xu, Z.L. Wang, Nano Lett. 6 (2006) 2768.
[12] Z.L. Wang, Adv. Funct. Mater. 18 (2008) 1.
[13] M.Y. Choi, D. Choi, M.J. Jin, I. Kim, S.H. Kim, J.Y. Choi, S.Y. Lee, J.M. Kim, S.W. Kim, Adv. Mater. 21 (2009) 1.
[14] E.D. Palik, Handbook of Optical Constants of Solids, Academic Press, San Diego, 1985.
[15] H.X. Yuan, B.X. Xu, B. Lukıyanchuk, T.C. Chong, Appl. Phys. A 89 (2007) 397.
[16] T. Xu, C. Wang, C. Du, X. Luo, Opt. Express 16 (2008) 4753.
[17] R. Gordon, A.G. Brolo, Opt. Express 13 (2005) 1933.
[18] M. Benyoucef, Institute for Integrative Nanosciences, IFW-Dresden, Private communication.